Iron and zirconium modified *luffa* fibre as an effective bioadsorbent to remove arsenic from drinking water

Thi Thuc Quyen Nguyen, Paripurnanda Loganathan, Tien Vinh Nguyen*,
Saravanamuthu Vigneswaran, Huu Hao Ngo
Faculty of Engineering and IT, University of Technology Sydney (UTS), Sydney, Australia
* Corresponding author: Tien Vinh Nguyen, Email: Tien.Nguyen@uts.edu.au; Tel: 61-2-95142620; Fax: 61-2-95147803

Abstract:

Porous *luffa* plant fibre (LF) was grafted with Fe and Zr, and the ability of the fabricated adsorbents to remove arsenate (As(V)) from water was investigated in batch and column adsorption experiments. The Langmuir adsorption capacity (mg g^{-1}) at pH 7 of LF was found to be 0.035, which increased to 2.55 and 2.89 after being grafted with Fe (FLF-3) and Zr (ZLF-3), respectively. Grafting with Fe and Zr increased the zeta potential and zero point of charge (ZPC) of LF (from pH 3.9 to 7.4 for Fe grafting and to 7.6 for Zr grafting), due to chemical bonding of the metals, possibly with the hydroxyl and carboxylic groups in LF as indicated in FTIR peaks. Zeta potential and ZPC decreased after As adsorption owing to inner-sphere complexation mechanism of adsorption. The increase of pH from 3 to 10 progressively reduced the adsorbents' adsorption capacity. Co-existing anions weakened the As(V) removal efficiency in the order, $PO_4^{3-} > SiO_3^{2-} > CO_3^{2-} > SO_4^{2-}$. Adsorption kinetics data fitted well to the Weber and Morris model, which revealed initial fast and subsequent slow rates of intra-particle As diffusion into the bigger pores and smaller pores, respectively. Column adsorption data fitted well to the Thomas model with the predicted adsorption capacities in the same order as in the batch adsorption experiment (ZLF-3 > FLF-3 > LF).

Keywords: *Arsenic adsorption; luffa fibre; iron modification; zirconium modification; drinking water treatment*

1. Introduction

Arsenic (As) is classified as a Class I human carcinogen because it is very toxic to people's health through the food chain and drinking water (Niazi et al., 2018). High doses of inorganic As cause a number of diseases related to the skin, lungs, and other organs such as vascular disease, renal disease, neurological problems, cardiovascular disease, and chronic lung disease (Berg et al., 2007; Mohan and Pittman, 2007). Two of the most toxic species of As in natural aqueous systems are trivalent (arsenite, As(III)) and pentavalent (arsenate, As(V)) ions (Berg, 2007). Generally, As(III) exists under mildly reducing conditions in the non-ionised form (H_3AsO_3) at pH < 9 and changes to ionised form ($HAsO_3^{2-}$) at pH > 9. While As(V) predominantly presents in oxidising conditions and exists in the ionised form ($H_2AsO_4^-$, $HAsO_4^{2-}$, AsO_4^{3-}) in a wide range of pH (pH 2 - 14). As in water is derived from both natural and anthropogenic sources. The major industrial processes that lead to As contamination are smelting of non-ferrous metals, combustion of fossil fuels, and manufacture and use of arsenical pesticides and wood preservatives. In nature, As could be found in minerals (e.g. pyrite) and hydrothermal veins (Søgaard, 2014), which on weathering release As to surface and ground waters and sediments. The most common As concentration of highly contaminated groundwater sources is around 0.1-0.5 mg L^{-1}, which is much higher than the WHO's guideline on drinking water for As (0.01 mg L^{-1}) (Nguyen et al., 2020a).

Because As is very dangerous to humans, scientists have implemented various strategies to remove As from drinking water. As well as the As removal efficiency feature of these methods, their cost-effectiveness, sustainability, and environmental-friendliness are prominent concerns. Among the numerous As removal techniques such as coagulation, adsorption, ion exchange, and membrane separation, adsorption is an efficient, cost-effective, and relatively easy-to-use method with minimum waste generation (Mohan and Pittman, 2007). Several

natural and synthetic adsorbents have been explored and used widely. Low-cost adsorbents consist of natural materials such as manganese ore, goethite, pisolite, red mud, dry plant materials, etc (Chiban, 2012; Mohan and Pittman, 2007). Of these, adsorbents derived from plants have been considered promising media for removing pollutants from water because of their environmental friendliness, low cost, local availability, and sustainability (Abu-El-Halawa et al., 2003; Chiban et al., 2009).

Luffa fibre (LF) is a material derived from the *luffa* plant. The *luffa* plant belongs to the family of *Cucurbitaceae* and is widespread in subtropical and tropical areas, especially in Southeast Asia, South Asia, Africa, and South America (Chen et al., 2014; Wang et al., 2017). The internal structure of old cylindrical *luffa* is a fibre-connecting porous and open-cell foam material with the pattern of branched fibres (Chen et al., 2014). It contains cellulose/hemicellulose, lignin, proteins, amino acids, polypeptides, glycosides, and other inorganic compounds (Chen et al., 2014). *Luffa* is used widely as food (the young and fresh variety), daily household cleaning material, and as a packaging material (the old and dry variety) (Chen et al., 2014; Wang et al., 2017). In the environmental field, it can be used in many applications. For example, natural *luffa* cylindrical fibre has been trialled as an adsorbent to remove methylene blue dye, phenol, and lead from aqueous solutions (Abdelwahab and Amin, 2013; Adewuyi and Pereira, 2017; Demir et al., 2008). However, it has not been used as an adsorbent for removing As from drinking water.

In this research, LF with and without chemical modification was used to remove As(V) from water. To enhance the adsorption capacity of the original LF, the LF material was modified by grafting it with iron (Fe) and zirconium (Zr) separately. These metals were selected for grafting for two reasons: firstly, high affinity of their oxides/hydroxides to As adsorption; and secondly, their safety as regards to human health (Nguyen et al., 2020b). The hydroxyl and carboxylic groups on the surface of LF can specifically adsorb Fe and Zr which are known to have high adsorption capacity towards As(V) (Adewuyi and Pereira, 2017;

Gupta et al., 2013; Kalaruban et al., 2019; Nguyen et al., 2020b). The performance of original and modified LF on As(V) removal from synthetic water was evaluated through batch and column adsorption studies. The effects of pH and coexisting anions on the adsorption process were also evaluated. The novelty of this present study is that it is the first to compare As removal performance of a bioadsorbent originating from a commonly cultivated plant (*luffa*) before and after chemical modification with two metals, Fe and Zr, having very high As adsorption capacities in both batch and column-based experiments. Zeta potential and FTIR measurements are used to explain the Fe and Zr complexation on LF and adsorption of As on the metals-grafted LF. Previously, column-based studies that have direct relevance to practical treatment-plant operations have rarely been reported for As adsorption by bioadsorbents.

2. Material and Methods

2.1 Feed solution

A synthetic stock solution was prepared by dissolving 4.165 mg sodium arsenate ($Na_2HAsO_4 \cdot 7H_2O$) in 1 L Milli-Q water to obtain a concentration of 1 mg As(V) L^{-1}. The stock solution was diluted to the desired concentration of 0.5 mg L^{-1} for batch studies and 0.1 mg L^{-1} for fluidised column studies. These concentrations are typical of As contaminated groundwaters in many countries. The ionic strength of the solution in batch studies was maintained at 1 mM $NaNO_3$. The solution pH was also adjusted to 7.0 ± 0.2 (except from 3 to 10 in the study on the effect of pH on As adsorption) by adding 0.1 M HNO_3 or 0.1 M NaOH.

2.2 Luffa material

2.2.1 Original material

The raw dry *luffa* appears as a cylindrical sponge column supported by a fibrous network. The *luffa* column has four major areas, these being the inner surface, outer surface, interlayer, and core. They grow in different directions, for instance the longitude,

104 circumferential, and radial directions. LFs include small empty channels with an internal
105 diameter of 1-10 µm. Old *luffa* fruits with dark brown peel were collected from a household
106 in My Duc rural district, Hanoi, Vietnam. It was naturally sun-dried and the *luffa* fibre (in the
107 form of cylinder sponge) was separated. The LF was cut into small pieces manually and
108 crushed to the size of 0.5-1 mm using a grinder. It was then washed by deionised distilled
109 water, dried at 70 ^{0}C, and stored in airtight containers.
110
111 *2.2.2 Modified materials*
112 The procedure employed by Gu et al. (2005) was modified and used to prepare iron
113 (Fe)-grafted *luffa* fibre (FLF) and zirconium (Zr)-grafted *luffa* fibre (ZLF). The modification
114 method comprised the following three steps.
115 Step 1: 10 g dried LF of size 0.5-1 mm was added into a 150 mL solution of 0.1 M
116 ferrous chloride tetrahydrate ($FeCl_2.4H_2O$). The pH of the suspension reduced to
117 approximately 2.0 probably due to the hydrolysis of Fe. 0.1 M NaOH was added to the
118 solution to raise the pH to 4.2 - 4.5, and the mixture was agitated at 120 rpm for 24 h at room
119 temperature (25 ± 1 °C).
120 Step 2: FLF produced in Step 1 was separated from the above mixture and dried at 70
121 °C for 24 h. The material was then washed with Milli-Q water till the brown coloured fraction
122 (excess iron) was removed, and the remaining fibre dried again at 70 °C for 24 h to produce
123 FLF-1.
124 Step 3: To enhance the degree of grafting, the FLF-1 was grafted once and then twice
125 more using the above procedure to produce FLF-2 and FLF-3, respectively. After cooling, all
126 FLFs were stored in airtight containers for testing.
127 ZLF-1, ZLF-2, and ZLF-3 were also produced using the same methods except by
128 mixing LF with 0.1 M zirconyl chloride octahydrate ($ZrOCl_2.8H_2O$) instead of ferrous

chloride tetrahydrate. When the Zr salt was added the pH reduced to around 2.0 and NaOH was added to raise the pH to 4.2-4.5 as in the case of Fe salt addition described above.

2.3 Comparison of the As adsorption capacity of different Luffa modifications

In order to compare the adsorption capability of new adsorbents produced from the two kinds of grafting agents and grafting cycles, three different amounts of modified LFs (0.02, 0.05 and 0.07 g) were mixed with 100 mL As(V) solution of 0.5 mg L^{-1} and shaken at 120 rpm for 24 h. The initial pH and ionic strength of the solution were 7.0 ± 0.2 and 1 mM $NaNO_3$, respectively. After shaking the suspensions, the supernatant was filtered using 0.45 µm filters, and the filtrates were analysed for As using an ICP-MS instrument (Agilent Technologies 7900 ICP-MS). The results (presented in Section 3.1) demonstrated that FLF-3 and ZLF-3, which were LF grafted three times with Fe and Zr, had the highest As adsorption capacity. Consequently, FLF-3 and ZLF-3 were chosen for the subsequent studies, including their characterisation.

2.4 Material characterisation

The morphology and elemental composition of pristine LF, FLF-3, and ZLF-3 were determined using scanning electron microscopy (SEM) and energy-dispersive X-ray spectroscopy (EDS) (Quanta-650 instrument). The main functional groups' presence on the material surface was measured by Fourier transform infrared spectroscopy (FTIR, Nicolet iS5 FT-IR Spectrometer). BET surface area and Zeta potential were determined using N_2 adsorption isotherm at 77 K with a Micromeritics absorptiometer (Accu Pyr II 1340. V1.02) at 77 K and Nano ZS Zen 3600, respectively. The Barrett-Joyner-Halenda (BJH) method served to calculate the total pore volume, pore size distribution and average pore diameter (Kalaruban et al., 2019). The mineralogy was determined using a XRD Empyrean (Netherlands) diffractometer on

154 powder samples of the adsorbents. The X-ray diffractometer was equipped with a Cu target
155 operated at 45 kV and 40 mA with a setting of 5–80 º (2θ), step time 2 º/min.
156 The elemental composition of LF and modified LFs were also determined by chemical
157 analysis using strong acid digestion. Here, 0.1 g sample was added into 100 mL mixed
158 solution of 2M HNO_3 and 1M HCl (1:1 volume ratio) and shaken for 4 h at 50 ^{0}C
159 (modification of the method employed by Kalaruban et al. (2016)). The suspensions were
160 filtered, and the filtrate was analysed for heavy metals using Agilent Technologies 4100 MP-
161 AES instrument.
162
163 *2.5 Batch adsorption studies*
164 The equilibrium adsorption study was conducted by mixing predetermined amounts of
165 adsorbents (1-5 g LF and 0.003-0.07 g of modified FLF-3 and ZLF-3) with 100 mL of 0.5 mg
166 As(V) L^{-1} in 250 mL flasks and shaking them at 120 rpm for 24 h. At the end of this period,
167 the suspensions were filtered, and As in the filtrate was analysed as described earlier. The pH
168 of the solution was kept constant at 7.0 ± 0.2 by checking the pH after 2-3 h and adjusting
169 back to the original value. This pH was selected for adsorption studies because most of the As
170 contaminated natural surface and ground waters had approximately neutral pH (Berg, 2007;
171 Mohan and Pittman, 2007). Initially, the pH increased during adsorption probably due to
172 exchange of As(V) anions with hydroxide groups attached to the Fe and Zr by ligand
173 exchange, leading to increased hydroxide ion concentration in solution (Ren et al., 2011). The
174 Langmuir, Freundlich and Temkin models were then used to model the experimental data.
175 The adsorption kinetics was carried out by mixing 1 g LF or 0.02 g FLF-3 or ZLF-3
176 with 100 mL of 0.5 mg As(V) L^{-1} in 250 mL flasks and shaking the flasks at 120 rpm. The
177 samples were collected at different adsorption periods, from 5 min to 24 h, and As(V)
178 concentration in solution was analysed as described in the equilibrium experiment. The

179 experimental data were then modelled using pseudo-first order (PFO), pseudo-second order
180 (PSO), Elovich, and Weber and Morris models.
181 The analysis of the pH influence on As(V) adsorption by LF and modified LFs was
182 carried out by adjusting the pH of feed solution from 3 to 10. The dose of adsorbents was kept
183 constant at 10 g L^{-1} for LF and 0.2 g L^{-1} for modified LFs and the initial As concentration was
184 0.5 mg As(V) L^{-1}. The experiments were conducted using a method similar to the one
185 described for the equilibrium adsorption experiment. The final pHs were measured at the end
186 of the adsorption period.
187 The sodium salts of phosphate (PO_4^{3-}), sulphate (SO_4^{2-}), silicate (SiO_3^{2-}) and carbonate
188 (CO_3^{2-}) at concentrations 0.1 and 10 mg L^{-1} were also added separately and together into
189 As(V) solution of 0.5 mg L^{-1}. This was done to evaluate the influence of coexisting anions on
190 As(V) adsorption capacity of LF and modified LFs. In this set of experiments, the same
191 predetermined amounts of adsorbents were used (30 g L^{-1} of LF and 0.3 g L^{-1} of modified
192 LFs). As with the batch experiments, the pH of the solution was kept constant.
193
194 *2.6 Fluidised-bed adsorption studies*
195 Fluidised-bed adsorption experiments were conducted using acrylic glass tubes. The
196 adsorbents were filled in the columns to two bed-heights (H) of 15 cm and 30 cm. Cotton
197 balls were placed at the top and bottom of the column to keep the adsorbents in place without
198 changing the bed heights. In total there were six columns in this set of experiments,
199 corresponding to 2 columns (at 2 different heights) for each of the 3 adsorbents. Synthetic
200 water containing As(V) of 0.1 mg L^{-1} was pumped by a dosing pump (Master-Flux L/S) in the
201 up-flow mode through the columns at a constant flow rate of 47 mL h^{-1} (corresponding to 0.6
202 m h^{-1}). The effluent samples were collected at 2 h intervals in the first 24 h, and then once a
203 day until the column was almost saturated with As. The experimental data were modelled
204 using the Thomas model.

205

206 **3. Results and discussion**

207 *3.1 Comparison of the As(V) adsorption capacity of different modified LFs*

208 The experimental results showed that the As(V) adsorption capacity of the original LF
209 did improve significantly after Fe and Zr modifications (Fig. 1). Moreover, the increase in the
210 number of grafting cycles also increased the As(V) adsorption capacity. At a dose of 0.2 g L^{-1},
211 As(V) removal efficiency of ZLF-1 was 30%, then it rose to 45% with ZLF-2 and 78% with
212 ZLF-3. In comparison with the original LF, the As(V) removal efficiency of ZLFs was 15 to
213 48% higher. The same trend was also observed with FLFs. This improvement can be
214 explained by the increasing amount of Fe and Zr on the surface of *luffa* through the multi-
215 cycle grafting process, as demonstrated by EDS and chemical analysis results (discussed later
216 in the paper). Due to the highest As(V) removal efficiency of FLF-3 and ZLF-3 in comparison
217 with other modifications cycles, they were used in the subsequent experiments.

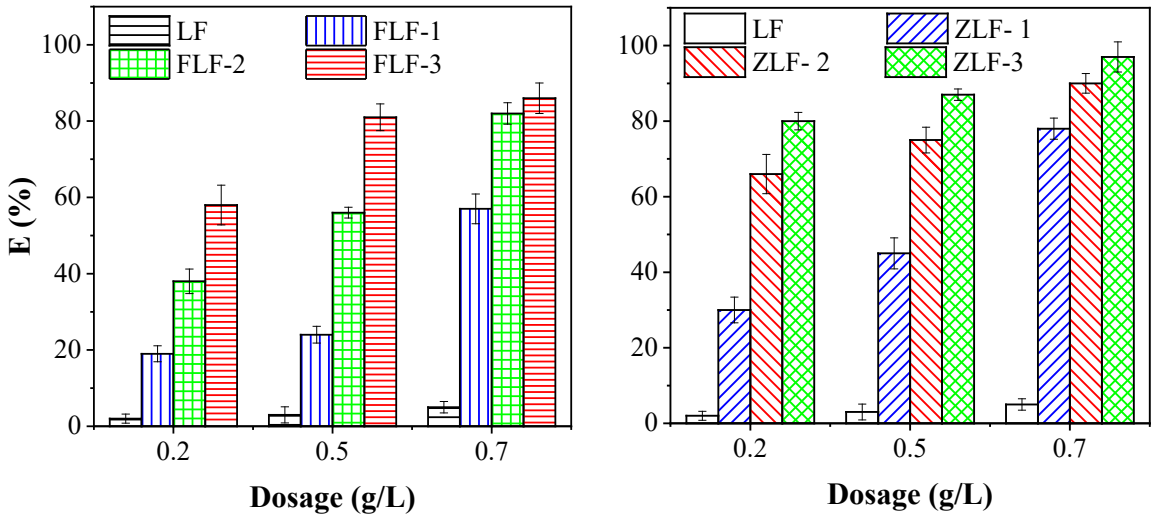

(a) (b)

Fig. 1. The As removal efficiency percentage (E%) comparison of the modification methods, (a) Fe grafted-LF and (b) Zr grafted-LF

3.2 Characteristics of adsorbents

The SEM images clearly showed the fibre structure of LF (Fig. S1, Supplementary data). These images also displayed extremely different surfaces before and after the modification of LFs. While original LF possessed a relatively flat, smooth, homogeneous surface (Wang et al., 2017) the modification process caused a reduction in the homogeneity. The modified LFs developed an irregular surface with a rough microstructure formation on the surface as reported for LF after chemical washing by (Wang et al., 2017). Chaudhry et al. (2017) reported that when Fe/Zr oxides were coated on sand, the surface became very irregular and porous and ascribed this as due to the formation of amorphous and porous Fe/Zr oxides. Chemical treatment during Fe and Zr grafting (acidity production and subsequent alkali addition to neutralisation of acidity) might have removed the gummy/waxy materials in LF to expose the rough surface as stated by Stella and Vijayalakshmi (2019). The porous structure of the modified LFs is consistent with the increase in the BET surface area and pore volume presented in the section below. No visible change occurred in the surface appearance

237 of the adsorbents after As adsorption. This could be due to the very low concentration of
238 As(V) on the LF surface.
239 The EDS analysis was carried out to determine the concentrations of the grafting agents
240 in LF. The EDS mapping clearly showed that Fe and Zr are concentrated on LF surface with
241 the former spread over a larger surface (Fig. S1). The concentrations of Fe and Zr in the
242 respective metals grafted LF determined from the spectra are 6.09 and 4.95% (Fig. S1). The
243 chemical analysis also revealed the notable increase of Fe and Zr amounts after each grafting
244 cycle. The highest percentages of the grafting agent's metals by the chemical analysis were 5.4
245 % Fe for FLF-3 and 5.3 % Zr for ZLF-3, compared to 2.9 % Fe and 2.0 % Zr for FLF-1 and
246 ZLF-1, respectively. The percentage of Fe and Zr after As adsorption remained nearly the same,
247 indicating that these metals did not leak into the solution during the adsorption process.
248 The BET surface area and pore volume of LF were quite small (0.61 $m^2 g^{-1}$ and 0.0034
249 $cm^3 g^{-1}$) (Table S1, Fig. S2a). These values increased considerably after the grafting process.
250 The BET surface area of FLF-3 and ZLF-3 were 6.7 $m^2 g^{-1}$ and 10.7 $m^2 g^{-1}$, respectively,
251 which are 11 and 18 times the value of the original LF. However, the BET surface areas of the
252 modified LFs are still small in comparison with most other adsorbents (Mohan and Pittman,
253 2007). The BJH total pore volume ($cm^3 g^{-1}$) of FLF-3 and ZLF-3 are 0.006 - 0.007 compared
254 to 0.003 - 0.004 of LF (Table S1). Both modified and unmodified LFs had mainly mesopores
255 (> 95% mesopores (2 - 50 nm)) and < 5% micropores (< 2 nm) (Fig. S2b). Adewuyi and
256 Pereira (2017) also reported that the raw luffa fibres had mainly mesopores with a range of
257 pores of 10-30 nm sizes. The average pore size of LF is 16 - 27 nm, whereas that of FLF-3
258 and ZLF-3 are 3.3 - 4.9 and 3.5 - 5.0 nm, respectively. The cumulative pore volume increased
259 at a faster rate with decrease in pore size from 4 nm for FLF-3 and ZLF-3, but this was not the
260 case with LF (Fig. S2b).
261 XRD analysis showed the presence of cellulose in the original and metals grafted LFs
262 (Fig. S3a). The peaks at 2θ = 15 - 16, 22.6, and 34.4 are characteristics of commercial

263 cellulose (Stella and Vijayalakshmi, 2019). Hemicellulose and lignin in the samples could not
264 be identified in the analysis because they are non-crystalline (amorphous) compounds
265 (Hideno, 2016) and XRD can only identify crystalline minerals.

266 The chemical components of LF are reported to be mainly cellulose (60 - 66%),
267 hemicellulose (17 -22%), and lignin (11 - 15%), which have hydroxyl and carboxyl chemical
268 groups with a strong affinity to bind with heavy metals (Adewuyi and Pereira, 2017; Siqueira
269 et al., 2010). Adewuyi and Pereira (2017) reported that the principal mechanisms of Pb
270 adsorption on *luffa* fibres are ion exchange of the Pb with protons in the carboxylic and hydroxyl
271 functional groups in cellulose and hemicellulose and H-bonding between Pb hydroxide species
272 and these functional groups. Similar mechanisms of adsorption would have occurred for other
273 heavy metals including Fe and Zr in this study. The FTIR pattern of LF shows peaks at 3690
274 cm^{-1} and 1640 cm^{-1} corresponding to -O-H stretching and bending, respectively, which are the
275 chemical bands of cellulose (Fig. S3b) (Petit and Puskar, 2018; Siqueira et al., 2010). The peaks
276 at 1710 cm^{-1} is assigned to -C=O functional group in the components of hemicellulose and
277 lignin (Siqueira et al., 2010). The peak at 1053 cm^{-1} revealed the presence of =C-O group in
278 either phenol or ester groups (Adewuyi and Pereira, 2017; Siqueira et al., 2010). The intense
279 peak from 971 to 1127 cm^{-1} for Fe grafted LFs is the bending vibration of hydroxyl groups of
280 Fe (hydr)oxides in LF (Zhang et al., 2009). The peaks at 992 and 1506 cm^{-1} for the ZLF-3 are
281 associated with -Zr-O and -Zr-OH bonds, respectively (Velazquez-Jimenez et al., 2014).

282 The peaks from 971 to 1127 cm^{-1} of the FLF-3 and 992 cm^{-1} of ZLF-3 adsorbents
283 reduced in size after As(V) adsorption, and no new peak appeared in the FTIR diagram (Fig.
284 S3b). This indicates that As(V) reacted only with the available functional groups of the
285 modified adsorbents and not formed any new compounds. Zhang et al. (2009) also reported
286 that these peaks (971 to 1127 cm^{-1}) weakened when As(V) adsorbed on Fe oxide and
287 explained this as being due to As(V) forming a surface complex with Fe in the adsorbent. In
288 the case of ZLF-3, the zirconyl ions on the surface of the Zr grafted LF adsorbent would have

chemically adsorbed As(V) (Daus et al., 2004). The FTIR results suggest that chemical adsorption of As(V) on Fe and Zr sites in LF might be the primary mechanism of As(V) adsorption on FLF and ZLF.

Fig. 2 shows the zeta potential (ZP) pattern of the three adsorbents before and after As(V) adsorption. The ZP value of FLF-3 and ZLF-3 were much higher than that of LF due to the impregnation of the positively charged Fe and Zr on LF's surface. The zero points of charge (pH at which the net surface charge is zero) of LF, FLF-3, and ZLF-3 were 3.9, 7.4, and 7.6, respectively. The ZP of these adsorbents decreased when pH was increased and also after As(V) adsorption. This is because of the specific adsorption of the increased amounts of OH^- at increased pHs as well as the specific adsorption, i.e. inner-sphere complexation (Loganathan et al., 2014) of the negatively charged arsenic ionic species (Mondal et al., 2007). LF also contains cellulose chains with hydroxyl groups that can bind with As(V) anions by hydrogen bonding and remove it from the solution (Elias et al., 2012; Fang et al., 2014). The positive charges produced as a result of Fe and Zr impregnation would have also adsorbed the negatively charged As(V) by electrostatic forces (physical adsorption or outer-sphere complexation) (Loganathan et al., 2014). The fact that the positive ZP decreased after As(V) adsorption indicates that the adsorption mechanism of modified LFs also included chemical process (inner-sphere complexation). Others have also reported both physical and chemical processes operating for the adsorption of As(V) on Fe (Kalaruban et al., 2019), and Zr (Velazquez-Jimenez et al., 2014) -grafted organic carbon-based adsorbents.

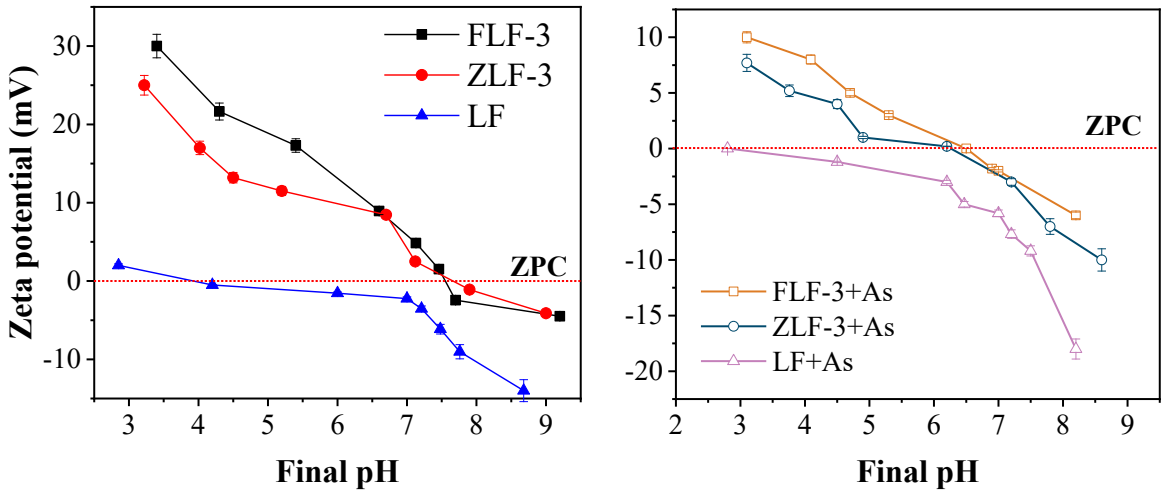

(a) (b)

Fig. 2. The zeta potential of LF and modified LFs before (a) and after (b) As(V) adsorption

3.3 Batch adsorption studies

3.3.1 Equilibrium adsorption

Fig. 3 illustrates the equilibrium adsorption of As(V) on LF and modified LFs. The data were evaluated using nonlinear forms of the Langmuir, Freundlich, and Temkin models. The adsorption data fitted well to all three adsorption models, with the Temkin model being the best-fitted model for the data of LF. The R^2 values for all model fittings were >0.88, indicating that the fits were very highly significant (probability level = 0.001) (Preece et al., 1982) (Table S2). The Langmuir maximum As(V) adsorption capacity (q_m) of LF was 0.035 mg g^{-1}, and it increased remarkably after modification. The Langmuir adsorption capacities of FLF-3 and ZLF-3 were 2.55 mg g^{-1} and 2.89 mg g^{-1}, respectively (Table S2). These values are 70-80 times higher than that of the original LF. It clearly confirms the beneficial impact of the grafting process. The improvement of As(V) adsorption capacity is due to the strong adsorption of the anionic arsenic species onto Fe and Zr on the surface of the modified LFs, as explained by the FTIR and zeta potential data earlier. The Langmuir isotherm constant k_L is related to the strength of the interaction between the adsorbent and adsorbate (Kocherbitov and Arnebrant, 2010). The k_L value for the three adsorbents is in the order ZFL-3 > FLF-3 >

LF, which is the same order of q_m. This shows that grafting of Zr and Fe on LF not only increased the adsorption capacity, but also increased the energy of adsorption.

Furthermore, the favourable nature of As(V) adsorption on LFs was analysed using an essential feature of the Langmuir isotherm model. This is the dimensionless equilibrium parameter R_L as shown in the equation below.

$$R_L = \frac{1}{1+(1+K_L.C_0)} \quad [1]$$

The R_L values for all the adsorbents in this study are $0 < R_L < 1$ (LF 0.23, FLF-3 0.172, ZLF-3 0.051), indicating that the adsorption process is favourable (Demir et al., 2008).

Although the Freundlich constant k_f does not give the maximum As(V) adsorption capacity like the q_m parameter of the Langmuir model, it is related to the adsorption capacity (Dada, 2012). The model results showed that the k_f values ((mg g^{-1}) (L mg^{-1})$^{1/n}$) of FLF-3 and ZLF-3 are 3.020 and 3.851, respectively, which are 65 - 80 times higher than that of the unmodified LF (0.047) (Table S2). This is consistent with the q_m value differences between the adsorbents. The values of the Freundlich exponent n term for all the adsorbents were between 1 and 10 (LF 1.89, FLF-3 2.45, ZLF-3 3.32). Thus, the values for 1/n were between 0 and 1, indicating again a favourable sorption process, which is consistent with the conclusion made from the Langmuir model (Nguyen et al., 2020b).

The Temkin model is usually used for heterogeneous surface energy systems and chosen to evaluate the adsorption potentials of the adsorbent for adsorbates (Nguyen et al., 2020b). The Temkin isotherm equilibrium binding constant A_T (L g^{-1}) (464, 83 and 50 for ZLF-3, FLF-3 and LF, respectively) corresponding to maximum binding energy (Nayl et al., 2020), correlates well with the Langmuir constant k_L relating to the energy of adsorption (ZLF-3 > FLF-3 > LF) (Table S2). Temkin isotherm constant b_T (kJ mol^{-1}) is inversely related to the heat of adsorption B calculated from the equation $B = RT/b_T$ (unit of B, J mol^{-1}; R gas constant, 8.314 J mol^{-1} K^{-1}; T, absolute temperature K) (Dada, 2012). The positive values obtained for b_T suggest that the adsorption process is endothermic (Adeogun and Babu, 2015).

Others have also reported endothermic reaction for the adsorption of As(V) on Fe-Zr binary oxide coated sand (Chaudhry et al., 2017) and on natural laterite containing Fe oxides (Nguyen et al., 2020a) based on thermodynamic adsorption studies. The B value for LF of 0.009 J mol^{-1} is much lower than that for FLF-3 (0.586 J mol^{-1}) and ZLF-3 (0.543 J mol^{-1}), indicating that the thermal energy created in the adsorption reaction of LF is lower than that of the others.

The Langmuir adsorption capacity of LF is generally lower than those of other natural plants (Table 1). However, the adsorption capacity of LF improved remarkably after modification. The adsorption capacities of FLF-3 and ZLF-3 are comparable or much higher than those of many other chemically modified bioadsorbents (Table 1). Some As adsorption studies (Chiban et al., 2009; Daus et al., 2004; Zhang et al., 2013) were conducted at exceptionally high solution As concentrations up to 100 - 200 mg L^{-1} which are rarely found in contaminated groundwaters and therefore they are not included in Table 1. As(V) is mostly adsorbed by inner-sphere complexation onto the Fe and Zr hydroxy-oxides grafted on LF as shown by the zeta potential and FTIR data, and therefore, the As(V) adsorption capacity is not influenced by the surface area of the adsorbent matrix. In fact, there are many studies which have shown that adsorbents having very low surface area can have high adsorption capacities, because of certain constituents in the adsorbents having very high affinity towards As. For example, a study on As(V) adsorption by a Fe oxide grafted on biomass which had a very low surface area of 2 m^2 g^{-1} resulted in a Langmuir maximum adsorption capacity of 1.54 mg g^{-1} (Pokhrel and Viraraghavan, 2008). On the other hand, adsorbents having very high surface area do not necessarily have high adsorption capacity. This was demonstrated in a study of As(V) adsorption on granular activated carbon (GAC) and Fe grafted GAC, where GAC having a surface area of 1124 m^2 g^{-1} had a low adsorption capacity of 1.01 mg g^{-1}, whereas Fe-GAC with a surface area of 876 m^2 g^{-1} had an adsorption capacity of 1.43 mg g-1 (40% increase over GAC) (Kalaruban et al., 2019).

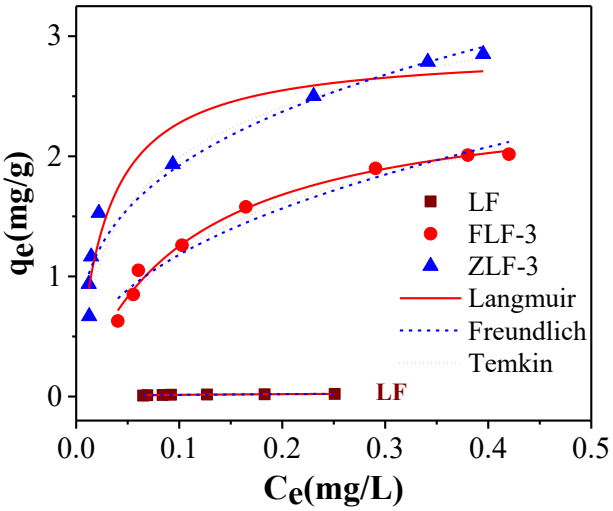

383

384 Fig. 3. Batch adsorption isotherms by LF and modified LFs

385

386 Table 1. Comparison of As(V) adsorption capacities of some bioadsorbents

Adsorbent	Solution pH	C_0 (mg L^{-1})*	Q (mg g^{-1})**	Reference
LF	7	0.5	0.035	This study
FLF-3	7	0.5	2.25	This study
ZLF-3	7	0.5	2.89	This study
Iron hydroxide modified activated carbon	7	0.025-1.5	0.37-1.25	Vitela-Rodriguez and Rangel-Mendez (2013)
Granular activated carbon	6	0.1	1.01	Kalaruban et al. (2019)
Iron coated granular activated carbon	6	0.1	1.43	Kalaruban et al. (2019)
Coal-based activated carbon	6	0.5	1.76	Li et al. (2014)
Manganese oxide-modified pine biochar	7	1-20	0.59, 0.91	Wang et al. (2015)
Iron oxide coated *A. niger* biomass	6	0.1	0.526	Pokhrel and Viraraghavan (2008)
Fish scale	6.8	0.333	0.0266	Rahaman et al. (2008)
Rice polish	4	0.1-1	0.147	Ranjan et al. (2009)
Anaerobic biomass	5	0.5-4	0.164	Chowdhury and Mulligan (2011)

387 *Initial As concentration, **Langmuir maximum adsorption capacity

388

389

3.3.2 Adsorption kinetics

The experimental data for the adsorption kinetics on LF, FLF-3, and ZLF-3 were fitted to non-linear PFO, PSO, Elovich models, and the linear Weber and Morris model (Fig. 4). The results show that As adsorption on ZLF-3 reached the fastest saturation within 60 min, (Table S3). LF and FLF-3 needed more time to reach the saturated point, 4 h and 6 h, respectively. The adsorption rate on all adsorbents during the initial period increased rapidly because a large number of adsorption sites were available for As(V) adsorption. As time progressed, it slowed down because of the gradual saturation of the adsorption sites before finally reaching an equilibrium state with no change in adsorption capacity. Between the PFO and PSO models, the latter fitted the data better for FLF-3 and ZFL-3, as revealed by the higher R^2 values (0.985, 0.986 for PSO; 0.894, 0.953 for PFO). In addition, the experimental maximum adsorption capacity (q_{exp}) was closer to the predicted adsorption capacity of the PSO model (q_e) than those for the PFO model for these modified LFs. This suggests that the main As(V) adsorption mechanism was chemical adsorption for the modified LFs (Kalaruban et al., 2019), as also found from the zeta potential data. The PSO adsorption rate constant (k_2, g mg^{-1} h^{-1}) of ZLF-3 (5.1) is higher than that of FLF-3 (0.8) (Table S3), indicating that it had a higher rate of adsorption than FLF-3. For the unmodified LF, the R^2 of the model fits to the data, and the q_{exp}/q_e difference between the two models was nearly the same. Therefore, the results could not suggest whether PSO or PFO is a better predictive model for LF adsorption and whether the adsorption process is chemical or not.

The Elovich model fitted well to the adsorption data of all three adsorbents (Fig. 4a). The α values of FLF-3 and ZLF-3 were much higher than that of LF, indicating that the initial rate of adsorption was increased significantly after modification. This phenomenon can be explained by the higher affinity of Fe and Zr modified LFs to As(V). The value of β (g mg^{-1}), the desorption constant, which is inversely related to the affinity of adsorbate to adsorbent

(Wang et al., 2015; Zhang et al., 2013) is much lower for FLF-3 (4) and ZLF-3 (6) than for LF (233) (Table S3), indicating that the modified LFs have stronger affinity to As(V) than LF.

Because LF consists of pores and channels, the Weber and Morris model was chosen to investigate the rate of As diffusion into this material through these pores/channels (Fig. 4b). The As(V) adsorption capacity of LF was too small, and therefore the change in adsorption rate could not be determined. For this reason, the Weber and Morris model fit to LF adsorption data was described by a single straight line. However, the As(V) adsorption process for FLF-3 and ZLF-3 appears to take place in two phases. The two phases were described by the two straight lines that fit the data in Fig. 4b. The data fit to the two straight lines for both the modified adsorbents are very highly significant with R^2 values > 0.960. The k_p values of the first set of straight lines (k_{p1}) were higher than the respective k_p values (k_{p2}) of the second set of straight lines, indicating that the intra-particle diffusion rates of As(V) into these adsorbents at short-term adsorption are faster than those at the long-term process. The faster rate is due to intra-particle diffusion of As into the larger sized pores of the absorbents (mostly > 4 nm, Fig. S2), and the slower rate is due to intra-particle diffusion of As into the smaller sized pores (mostly < 4 nm, Fig. S2). Kalaruban et al. (2019) also reported a good fit of data to the Weber and Morris model for the kinetics of adsorption of As on Fe-coated granular activated carbon (GAC) with two distinct straight lines. They considered that the two straight lines fit, indicating As diffusing initially (short-term process) through the mesopores in GAC and later (long-term process) through the micro-pores in GAC.

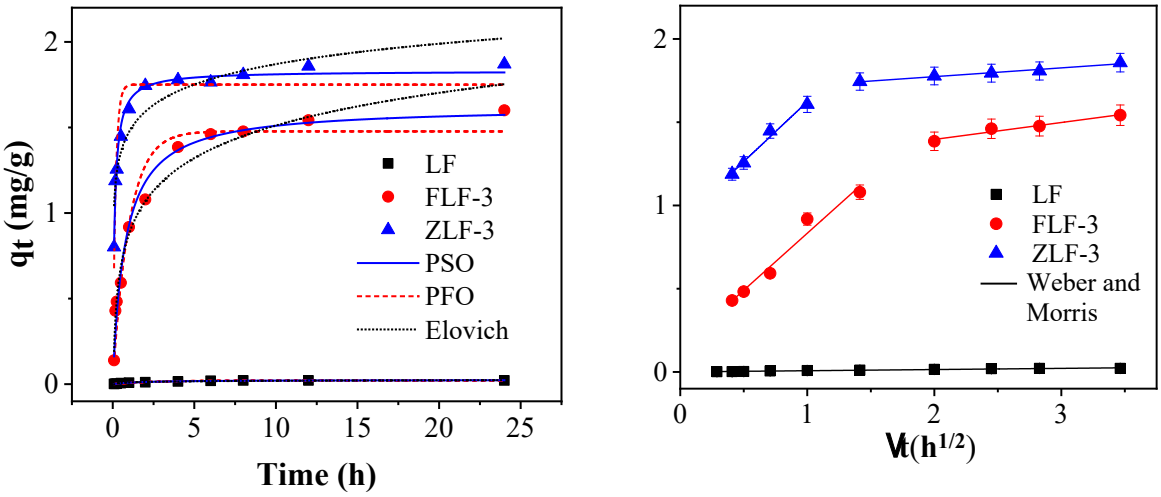

(a) (b)

Fig. 4. Batch kinetics adsorption by LF and modified LFs, (a) PFO, PSO and Elovich models and (b)Webber and Morris model

3.3.3 Influence of pH on As(V) adsorption

pH is one of the most important parameters of the adsorption process. It impacts the surface charge of the adsorbents, the extent of ionisation of the surface groups, the nature of the adsorbing ions, and finally influences the adsorption mechanisms (Firdaous et al., 2017). Fig. 5 shows the influence of pH on As(V) adsorption by LF, FLF-3, and ZLF-3. The As(V) adsorption efficiency of the three adsorbents declined when the pH rose from 3 to 10 (from 53 - 68%). This fall in adsorption capacity is due to the increase in the surface negative charges on the adsorbents as pH increases (as shown in the zeta potential diagram, Fig. 2), which is not favourable for the adsorption of the negatively charged As species. Additionally, the number of negative charges on the As species would have also increased with pH to aggravate this situation. Another reason is that the increasing concentration of hydroxyl ions at high pHs might have competed with As species for specific adsorption on the adsorbents.

The decline in As(V) adsorption capacity with rise in pH has also been reported by others. For example, for a granulated activated carbon (GAC) and iron grafted GAC, it was reported that the adsorption capacity continued to decrease with increase in pH from 6 to 8 (Kalaruban et al., 2019). For an iron-zirconium binary oxide adsorbent, it was shown that

As(V) adsorption efficiency continuously declined with increase in pH from 5 to 11 (Ren et al., 2011). Similarly, the adsorption of As(V) on iron and zirconium grafted manganese oxide ore decreased from pH 3 to 10 (Nguyen et al., 2020b). Also, for three types of iron oxide minerals and zero-valent Fe, As(V) adsorption decreased from pH 6 to 12 (Mamindy-Pajany et al., 2011).

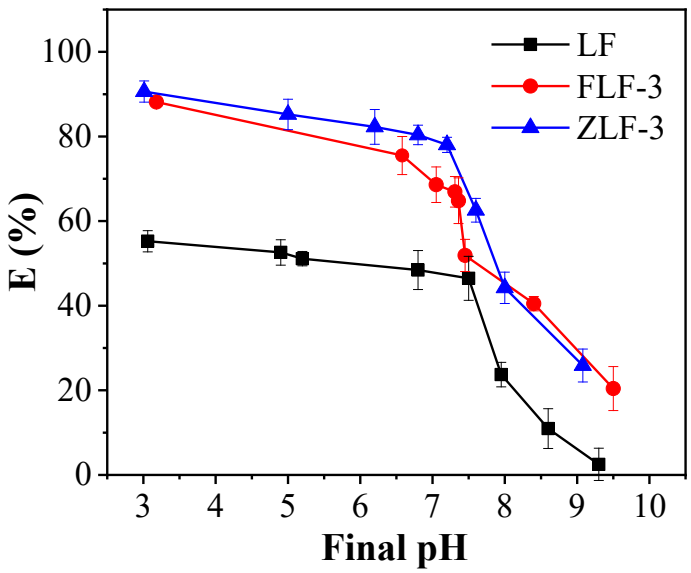

461

462 Fig. 5. Influence of pH on As(V) removal efficiency of LF (10 g L^{-1}), FLF-3 (0.2 g L^{-1}) and

463 ZLF-3 (0.2 g L^{-1})

464

465 *3.3.4 Effect of co-existing anions on As(V) adsorption*

466 In nature, many ions present in water, but some of them are able to interfere with the

467 uptake of As through competitive adsorption. Four typical anions PO_4^{3-}, SiO_3^{2-}, SO_4^{2-} and

468 CO_3^{2-}, which commonly co-exist with As in water, were selected to evaluate the influence of

469 co-existing anions on As(V) adsorption.

470 The results showed that the performance of the three adsorbents was affected depending

471 on the presence of co-existing anions and their concentrations. At the lower concentration (0.1

472 mg L^{-1}), the effect of SO_4^{2-} and CO_3^{2-} ions on As(V) removal efficiency was almost invisible,

473 while the influence of PO_4^{3-} and SiO_3^{2-} ions was remarkable (As removal reduced by 20-30%,

474 in the case of FLF-3). At the higher concentration (10 mg L^{-1}) of each ion, PO_4^{3-} and SiO_3^{2-}

475 ions impacted greatly on the As(V) removal efficiency (As removal reduced by 50-70%),

476 especially PO_4^{3-} because of their chemical similarities (Ren et al., 2011).

477 In general, the order of competition for adsorption is: $PO_4^{3-} > SiO_3^{2-} > CO_3^{2-} > SO_4^{2-}$.

478 The same order of competition was also reported by Nguyen et al. (2020a) for As(V)

479 adsorption by a natural laterite containing Fe oxides. The reason for PO_4^{3-} and SiO_3^{2-} having

higher competition than $CO_3^{2-} > SO_4^{2-}$ is that they are adsorbed mostly by inner sphere complexation onto the Fe and Zr in the adsorbent compared to the latter two ions which are adsorbed mostly by outer sphere complexation (Tuutijärvi et al., 2012). Inner sphere complexation leads to strong chemical adsorption usually involving ligand exchange mechanism (adsorbent surface OH groups exchanging with anions such as arsenate) (Loganathan et al., 2014; Ren et al., 2011). Tuutijärvi et al. (2012) reported that SO_4^{2-} and NO_3^- had negligible effect on As(V) adsorption by maghemite but PO_4^{3-} and SiO_3^{2-} had strong adverse effect. Gu et al. (2005) also reported that SO_4^{2-} did not affect As(V) adsorption by Fe grafted GAC, whereas PO_4^{3-} and SiO_3^{2-} did. Ren et al. (2011) observed that the adsorption of As(V) by Fe/Zr binary oxide was not affected by SO_4^{2-}, slightly by CO_3^{2-}, and severely by PO_4^{3-} and SiO_3^{2-}. Of the last two anions, the former was considered to compete more intensively with As(V) because they have similar molecular structure and located in the same group in periodic table (Ren et al., 2011; Zhang et al., 2009). Another similarity is that both are oxyanions and have similar types of ionic species at neutral pH ($H_2PO_4^-$, HPO_4^{2-} ; $H_2AO_4^-$, $HAsO_4^{2-}$) (Tuutijärvi et al., 2012).

The competitive ability of the co-existing anions was enhanced when all of them were present in the same solution. The presence of multiple anions in solution competed for a greater number of adsorption sites of As, thus leading to the significant decline in As(V) removal efficiency. This decreased from 40% to 90% as the mixed anions concentration increased from 0.1 mg L^{-1} to 10 mg L^{-1}.

3.4 Fluidised-bed studies

Fig. 6 depicts the As breakthrough curves of six columns. At the same initial As(V) concentration (C_o = 0.1 mg L^{-1}) and filtration velocity (Q = 47 mL h^{-1}), the breakthrough curves of LF were always steeper than those of FLF-3 and ZLF-3. It means that LF saturated faster than the others did. At the same bed height, the plateau of C_t/C_o of these columns

506 occurred at different periods and bed volumes (BV). For example, with the 15 cm columns,
507 the life cycle of LF was shortest, and the plateau of C_t/C_o occurred around 120 h (BV 479,
508 C_t/C_o = 0.99). Meanwhile FLF-3 and ZLF-3 operated for much longer, and the ratio C_t/C_o =
509 0.98 occurred approximately at 1824 h, BV 7281, and 2832 h, BV 11304, respectively. In the
510 case of 30 cm columns, a similar trend was also observed. For LF, C_t/C_o of 0.80 was reached
511 at BV = 239 (120 h) while for FLF-3 and ZLF-3, this C_t/C_o was reached at BV of 3640 (1824
512 h) and BV of 5652 (2832 h), respectively.

513 For each adsorbent, the higher column height became saturated after a longer time than
514 the shorter one. This is because the column packed with an adsorbent to a greater height had a
515 larger number of adsorption sites for As(V) adsorption. The longer operational time of the
516 column with greater height enables it to treat larger volumes of water to maintain As
517 concentration below the WHO recommended level of 0.01 mg L^{-1}. For instance, the 30 cm
518 column with ZLF-3 adsorbent treated 33 L of water to the WHO level compared to 6.8 L
519 water the 15 cm column treated. The corresponding volumes of water treated by LF columns
520 were 0.1 and 0.2 L, respectively.

521 The total amount of As(V) adsorption, q_{total} (mg), and column adsorption capacity, $q_{e,exp}$
522 (mg g^{-1}) in the fluidised-bed studies were calculated using the following equations (Kalaruban
523 et al., 2016):

524 $$q_{total} = Q.\int_{t=0}^{t=total}(C_o - C_t)dt \quad [2]$$

525 $$q_{e,exp} = \frac{q_{total}}{m} \quad [3]$$

526 where: Q is the filtration velocity, (L h^{-1}); C_o is the initial As(V) concentration (mg L^{-1});
527 and C_t is the As(V) concentration at time t (h), (mg L^{-1}).

528 The calculations showed that ZLF-3 had the highest As(V) adsorption capacities at both
529 the column heights (2.630 and 1.950 mg g^{-1} with H 15 and 30 cm columns, respectively),
530 followed by FLF-3 (1.237 and 1.031 mg g^{-1}) and LF (0.054 and 0.053 mg g^{-1}).

The Thomas model (equation 4, Kalaruban et al. (2016)) fitted well to the experimental data with values of $R^2 > 0.87$ (Fig. 6).

$$\ln\left(\frac{C_o}{C_t} - 1\right) = \frac{K_{Th} q_e m}{Q} - K_{Th} C_o t \quad [4]$$

where: K_{Th} is the Thomas rate constant ($L.h^{-1}.mg^{-1}$); q_e is the maximum solid-phase concentration of As ($mg\ g^{-1}$); and m is the mass of adsorbent (g).

The modelling results showed that the maximum As adsorption capacity of ZLF-3 was the highest (2.7 and 2.2 $mg\ g^{-1}$ for 15 cm and 30 cm height columns, respectively), while that of LF was the lowest (0.06 $mg\ g^{-1}$ for both column heights). The corresponding values of FLF-3 were 1.26 $mg\ g^{-1}$ and 1.10 $mg\ g^{-1}$, respectively.

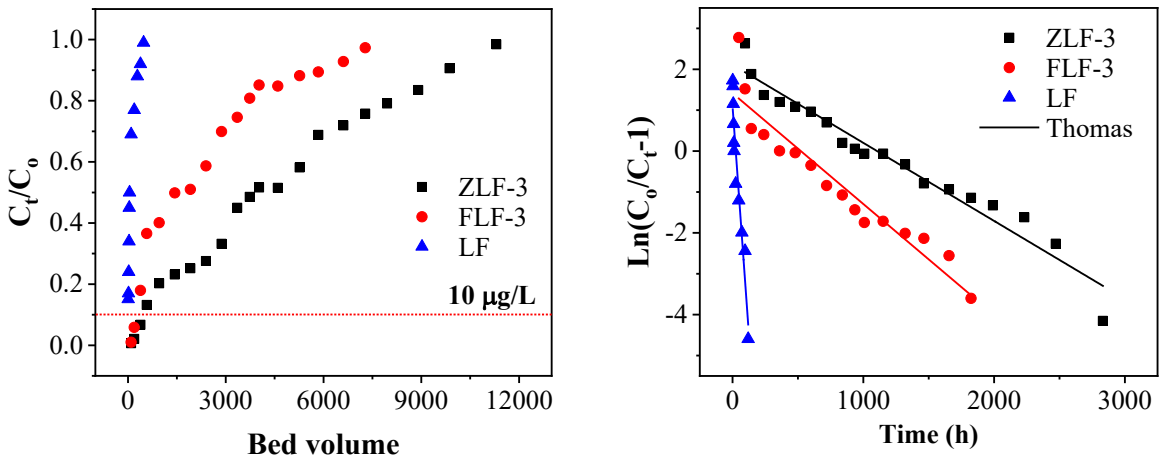

(a)

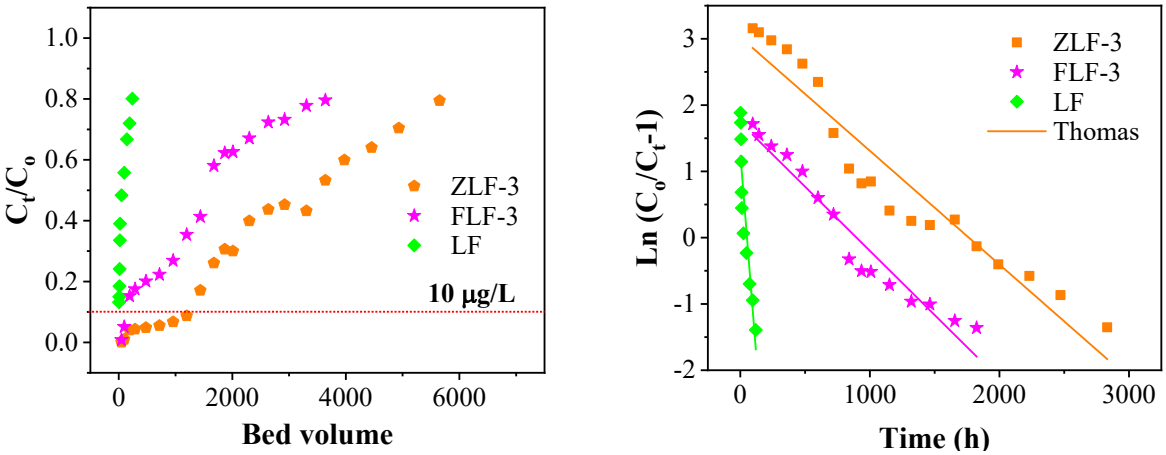

(b)

Fig. 6. The experimental breakthrough curves and Thomas model fit to data for As(V) removal at V = 0.047 L h^{-1}, C_o = 0.1 mg L^{-1} and H = 15 cm (a) or H = 30 cm (b)

3.5. Adsorption mechanism

Zeta potential data showed that when LF was modified with the positively charged Fe and Zr, the negative charges on LF significantly decreased at all pHs and reversed to positive values at pHs 4.0 to 7.5. FTIR data provided evidence that Fe and Zr were complexed with the hydroxyl and carboxylic groups mostly present in the cellulose component of LF. XRD data proved that cellulose was present in LF. The grafting of Fe and Zr produced significant amounts of these metals on the grafted product as shown in EDS mapping.

The positive charges generated on LF by Fe and Zr would have helped the adsorption of some As(V) by coulombic (electrostatic) forces leading to outer-sphere complexation. However, the major mechanism of As(V) adsorption is through inner-sphere complexation caused by ligand exchange of surface hydroxyl groups attached to Fe and Zr with As(V) species ($H_2AsO_4^-$; $HAsO_4^{2-}$) (Kalaruban et al., 2019; Mohan and Pittman, 2007; Nguyen et al., 2020b; Ren et al., 2011; Tuna et al., 2013). The evidence for this process is provided by the zeta potential data. The zeta potential of FLF and ZLF decreased and even became negative at pHs above 6.5 due to the negatively charged As(V) ions complexing with the Fe and Zr oxides/hydroxides. Because As(V) was adsorbed mainly by inner-sphere complexation the non-specifically adsorbing anions such as SO_4^{2-} and CO_3^{2-} were not able to compete well with As(V) for adsorption sites. The scheme of As(V) adsorption mechanism is illustrated in equations 5-8 below. Equations 5 and 6 are for $H_2AsO_4^-$, the dominant anionic species at pH 2-7, and equations 7 and 8 are for $HAsO_4^{2-}$, the dominant species at pH 7-12 (Ren et al., 2011). The complexation could have occurred by As(V) species acting as electron donors and the metal hydroxide groups acting as electron acceptors (Tuna et al., 2013). SEM images showed that Fe and Zr modifications exposed the pores and channels of the fibrous LF in the acidic conditions prevalent during the modification process which removed the gummy/waxy substances on the LF surface. The adsorption of As(V) on FLF and ZLF is not only on the planer surface of the adsorbent, but also inside these pores/channels by As(V) diffusion as demonstrated by Weber and Morris kinetic data analysis.

$$LF]\text{-}Fe\text{-}OH + H_2AsO_4^- \rightarrow LF]\text{-}Fe\text{-}H_2AsO_4^- + OH^- \quad [5]$$

$$LF]\text{-}Fe\text{-}OH + HAsO_4^{2-} \rightarrow LF]\text{-}Fe\text{-}HAsO_4^{2-} + OH^- \quad [6]$$

$$LF]\text{-}Zr\text{-}OH + H_2AsO_4^- \rightarrow LF]\text{-}Zr\text{-}H_2AsO_4^- + OH^- \quad [7]$$

$$LF]\text{-}Zr\text{-}OH + HAsO_4^{2-} \rightarrow LF]\text{-}Zr\text{-}HAsO_4^{2-} + OH^- \quad [8]$$

4. Conclusions

This study has demonstrated that porous fibres of the *luffa* plant (LF), which is found in most parts of the world, can be easily grafted with Fe and Zr, and the As(V) adsorption capacity can be increased by 70-80 times when compared to the unmodified raw LF. Grafting with Fe and Zr increased the zeta potential and zero point of charge (ZPC) of LF (from pH 3.9 to 7.4 for Fe-grafting and to 7.6 for Zr grafting), due to chemical bonding of the metals, possibly with the hydroxyl and carboxylic groups in LF as indicated in the FTIR pattern of peaks. Zeta potential and ZPC decreased after As adsorption owing to inner-sphere complexation mechanism of adsorption. The adsorption capacities of the grafted materials (2.55-2.89 mg g^{-1}) are higher than many of the other bioadsorbents. The Fe- and Zr-grafted LF are very promising cost-effective, and environmentally friendly bioadsorbents for the removal of As(V) from contaminated drinking water.

Supplementary data

Supplementary data to this article can be found online.

Acknowledgment

The project was funded by the Australian Government Department of Foreign Affairs and Trade's (DFAT) innovationXchange (iXc).

References

Abdelwahab, O., Amin, N.K., 2013. Adsorption of phenol from aqueous solutions by Luffa cylindrica fibers: Kinetics, isotherm and thermodynamic studies. Egypt. J. Aquat. Res. 39(4)215-223.

Abu-El-Halawa, R., Quora, R., Salim, R., 2003. Efficiency of Removal of Lead, Cadmium, Copper and Zinc from Aqueous Solutions Using Six Common Types of Plant Leaves. J.

606 Appl. Sci. 3, 79-84.
607 Adeogun, A.I., Babu, R.B., 2015. One-step synthesized calcium phosphate-based material for
608 the removal of alizarin S dye from aqueous solutions: isothermal, kinetics, and
609 thermodynamics studies. Appl. Nanosci. 1-13.
610 Adewuyi, A., Pereira, F.V., 2017. Underutilized Luffa cylindrica sponge: A local bio-adsorbent
611 for the removal of Pb(II) pollutant from water system. Beni-Suef Univ. J. Basic Appl. Sci.
612 6(2), 118-126.
613 Berg, M., 2007. Arsenic Contamination of Groundwater and Drinking Water in the Red River
614 Delta , Vietnam : Geochemical Investigations and Mitigation Measures: dis. dok. natur.
615 *Zurich, Schweiz.*
616 Berg, M., Stengel, C., Trang, P.T.K., Hung Viet, P., Sampson, M.L., Leng, M., Samreth, S.,
617 Fredericks, D., 2007. Magnitude of arsenic pollution in the Mekong and Red River Deltas
618 - Cambodia and Vietnam. Sci. Total Environ. 372(2-3), 413-425.
619 Chaudhry, S.A., Zaidi, Z., Siddiqui, S.I., 2017. Isotherm, kinetic and thermodynamics of arsenic
620 adsorption onto Iron-Zirconium Binary Oxide-Coated Sand (IZBOCS): Modelling and
621 process optimization. J. Mol. Liq. 229, 230-240.
622 Chen, Q., Shi, Q., Gorb, S.N., Li, Z., 2014. A multiscale study on the structural and mechanical
623 properties of the luffa sponge from Luffa cylindrica plant. J. Biomech. 47(6), 1332-1339.
624 Chiban, M., 2012. Application of low-cost adsorbents for arsenic removal: A review. J.
625 Environ. Chem. Ecotoxicol. 8, 1377-1383.
626 Chiban, M., Lehutu, G., Sinan, F., Carja, G., 2009. Arsenate removal by withania frutescens
627 plant from the south-western Morocco, in: Environmental Engineering and Management
628 Journal. 4(5), 91-102.
629 Chowdhury, M.R.I., Mulligan, C.N., 2011. Biosorption of arsenic from contaminated water by
630 anaerobic biomass. J. Hazard. Mater. 190(1), 486-492.
631 Dada, A.., 2012. Langmuir, Freundlich, Temkin and Dubinin–Radushkevich Isotherms Studies

of Equilibrium Sorption of Zn 2+ Unto Phosphoric Acid Modified Rice Husk. IOSR J. Appl. Chem. 3(1), 38-45.

Daus, B., Wennrich, R., Weiss, H., 2004. Sorption materials for arsenic removal from water: A comparative study. Water Res. 38(12), 2948-2954.

Demir, H., Top, A., Balköse, D., Ülkü, S., 2008. Dye adsorption behavior of Luffa cylindrica fibers. J. Hazard. Mater. 153(1), 389-394.

Elias, M., Wellner, A., Goldin-Azulay, K., Chabriere, E., Vorholt, J.A., Erb, T.J., Tawfik, D.S., 2012. The molecular basis of phosphate discrimination in arsenate-rich environments. Nature. 491.

Fang, Q., Chen, B., Lin, Y., Guan, Y., 2014. Aromatic and hydrophobic surfaces of wood-derived biochar enhance perchlorate adsorption via hydrogen bonding to oxygen-containing organic groups. Environ. Sci. Technol. 48(1), 279-288.

Firdaous, L., Fertin, B., Khelissa, O., Dhainaut, M., Nedjar, N., Chataigné, G., Ouhoud, L., Lutin, F., Dhulster, P., 2017. Adsorptive removal of polyphenols from an alfalfa white proteins concentrate: Adsorbent screening, adsorption kinetics and equilibrium study. Sep. Purif. Technol. 178, 29-39.

Gu, Z., Fang, J., Deng, B., 2005. Preparation and evaluation of adsorbents for arsenic removal. Environ. Sci. Technol. 39(10), 3833-3843.

Gupta, V.K., Agarwal, S., Singh, P., Pathania, D., 2013. Acrylic acid grafted cellulosic Luffa cylindrical fiber for the removal of dye and metal ions. Carbohydr. Polym. 98(1), 1214-1221.

Hideno, A., 2016. Comparison of the thermal degradation properties of crystalline and amorphous cellulose, as well as treated lignocellulosic biomass. BioResources. 11(3), 6309-6319.

Kalaruban, M., Loganathan, P., Nguyen, T.V., Nur, T., Hasan Johir, M.A., Nguyen, T.H., Trinh, M.V., Vigneswaran, S., 2019. Iron-impregnated granular activated carbon for arsenic

658 removal: Application to practical column filters. J. Environ. Manage. 239, 235-243.
659 Kalaruban, M., Loganathan, P., Shim, W.G., Kandasamy, J., Naidu, G., Nguyen, T.V.,
660 Vigneswaran, S., 2016. Removing nitrate from water using iron-modified Dowex 21K
661 XLT ion exchange resin: Batch and fluidised-bed adsorption studies. Sep. Purif. Technol.
662 158, 62-70.
663 Kocherbitov, V., Arnebrant, T., 2010. Hydration of lysozyme: The protein-protein interface and
664 the enthalpy-entropy compensation. Langmuir. 26(6), 3919-3922.
665 Li, W.G., Gong, X.J., Wang, K., Zhang, X.R., Fan, W.B., 2014. Adsorption characteristics of
666 arsenic from micro-polluted water by an innovative coal-based mesoporous activated
667 carbon. Bioresour. Technol. 165, 166-173.
668 Loganathan, P., Vigneswaran, S., Kandasamy, J., Bolan, N.S., 2014. Removal and recovery of
669 phosphate from water using sorption. Crit. Rev. Environ. Sci. Technol. 44(8), 847-907.
670 Mamindy-Pajany, Y., Hurel, C., Marmier, N., Roméo, M., 2011. Arsenic (V) adsorption from
671 aqueous solution onto goethite, hematite, magnetite and zero-valent iron: Effects of pH,
672 concentration and reversibility. Desalination. 281, 93-99.
673 Mohan, D., Pittman, C.U., 2007. Arsenic removal from water/wastewater using adsorbents-A
674 critical review. J. Hazard. Mater. 142(1-2), 1-53.
675 Mondal, P., Balomajumder, C., Mohanty, B., 2007. A laboratory study for the treatment of
676 arsenic, iron, and manganese bearing ground water using Fe3+ impregnated activated
677 carbon: Effects of shaking time, pH and temperature. J. Hazard. Mater. 144(1-2), 420-426.
678 Nayl, A.A., Ahmed, I.M., Abd-Elhamid, A.I., Aly, H.F., Attallah, M.F., 2020. Selective
679 sorption of 134Cs and 60Co radioisotopes using synthetic nanocopper ferrocyanide-SiO2
680 materials. Sep. Purif. Technol. 234, 116060.
681 Nguyen, T.H., Tran, H.N., Vu, H.A., Trinh, M.V., Nguyen, T.V., Loganathan, P., Vigneswaran,
682 S., Nguyen, T.M., Trinh, V.T., Vu, D.L., Nguyen, T.H.H., 2020a. Laterite as a low-cost
683 adsorbent in a sustainable decentralized filtration system to remove arsenic from

684 groundwater in Vietnam. Sci. Total Environ. 699, 134267.
685 Nguyen, T.T.Q., Loganathan, P., Nguyen, T.V., Vigneswaran, S., 2020b. Removing arsenic
686 from water with an original and modified natural manganese oxide ore: batch kinetic and
687 equilibrium adsorption studies. Environ. Sci. Pollut. Res. 1-13.
688 Niazi, N.K., Bibi, I., Shahid, M., Ok, Y.S., Burton, E.D., Wang, H., Shaheen, S.M., Rinklebe,
689 J., Lüttge, A., 2018. Arsenic removal by perilla leaf biochar in aqueous solutions and
690 groundwater: An integrated spectroscopic and microscopic examination. Environ. Pollut.
691 232, 31-41.
692 Petit, T., Puskar, L., 2018. FTIR spectroscopy of nanodiamonds: Methods and interpretation.
693 Diam. Relat. Mater. 89, 52-66.
694 Pokhrel, D., Viraraghavan, T., 2008. Arsenic removal from aqueous solution by iron oxide-
695 coated biomass: Common ion effects and thermodynamic analysis. Sep. Sci. Technol.
696 43(13), 3545-3562.
697 Preece, D.A., Little, T.M., Hills, F.J., 1982. Agricultural Experimentation: Design and
698 Analysis. Biometrics.
699 Rahaman, M.S., Basu, A., Islam, M.R., 2008. The removal of As(III) and As(V) from aqueous
700 solutions by waste materials. Bioresour. Technol. 99(8), 2815-2823.
701 Ranjan, D., Talat, M., Hasan, S.H., 2009. Biosorption of arsenic from aqueous solution using
702 agricultural residue “rice polish.” J. Hazard. Mater. 166(2), 1050-1059.
703 Ren, Z., Zhang, G., Paul Chen, J., 2011. Adsorptive removal of arsenic from water by an iron-
704 zirconium binary oxide adsorbent. J. Colloid Interface Sci. 358(1), 230-237.
705 Siqueira, G., Bras, J., Dufresne, A., 2010. Cellulosic bionanocomposites: A review of
706 preparation, properties and applications. Polymers (Basel). 5(2), 727-740.
707 Søgaard, E.G., 2014. Chemistry of Advanced Environmental Purification Processes of Water:
708 Fundamentals and Applications, Chemistry of Advanced Environmental Purification
709 Processes of Water: Fundamentals and Applications.

710 Stella, M.S., Vijayalakshmi, U., 2019. Influence of chemically modified Luffa on the
711 preparation of nanofiber and its biological evaluation for biomedical applications. J.
712 Biomed. Mater. Res. - Part A. 107(3), 610-620.
713 Tuna, A.Ö.A., özdemir, E., şimşek, E.B., Beker, U., 2013. Removal of As(V) from aqueous
714 solution by activated carbon-based hybrid adsorbents: Impact of experimental conditions.
715 Chem. Eng. J. 223, 116-128.
716 Tuutijärvi, T., Repo, E., Vahala, R., Sillanpää, M., Chen, G., 2012. Effect of competing anions
717 on arsenate adsorption onto maghemite nanoparticles. Chinese J. Chem. Eng. 20(3), 505-
718 514.
719 Velazquez-Jimenez, L.H., Hurt, R.H., Matos, J., Rangel-Mendez, J.R., 2014. Zirconium-carbon
720 hybrid sorbent for removal of fluoride from water: Oxalic acid mediated Zr(IV) assembly
721 and adsorption mechanism. Environ. Sci. Technol. 48(2), 1166-1174.
722 Vitela-Rodriguez, A.V., Rangel-Mendez, J.R., 2013. Arsenic removal by modified activated
723 carbons with iron hydro(oxide) nanoparticles. J. Environ. Manage. 114, 225-231.
724 Wang, S., Gao, B., Li, Y., Mosa, A., Zimmerman, A.R., Ma, L.Q., Harris, W.G., Migliaccio,
725 K.W., 2015. Manganese oxide-modified biochars: Preparation, characterization, and
726 sorption of arsenate and lead. Bioresour. Technol. 181, 13-17.
727 Wang, Z., Ma, H., Chu, B., Hsiao, B.S., 2017. Super-hydrophobic modification of porous
728 natural polymer “luffa sponge” for oil absorption. Polymer (Guildf). 126, 470-476.
729 Zhang, G., Liu, H., Liu, R., Qu, J., 2009. Adsorption behavior and mechanism of arsenate at
730 Fe-Mn binary oxide/water interface. J. Hazard. Mater. 168(2-3), 820-825.
731 Zhang, M., Gao, B., Varnoosfaderani, S., Hebard, A., Yao, Y., Inyang, M., 2013. Preparation
732 and characterization of a novel magnetic biochar for arsenic removal. Bioresour. Technol.
733 130, 457-432.